Inorg. Chem. **2003**, *42*, 4109–4116

The $CsLnMSe_3$ Semiconductors (Ln = Rare-Earth Element, Y; M = Zn, Cd, Hg)

Kwasi Mitchell, Fu Qiang Huang, Adam D. McFarland, Christy L. Haynes, Rebecca C. Somers, Richard P. Van Duyne, and James A. Ibers*

Department of Chemistry, Northwestern University, 2145 Sheridan Road, Evanston, Illinois 60208-3113

Received December 30, 2002

$CsLnCdSe_3$ (Ln = Ce, Pr, Sm, Gd, Tb, Dy, Y) and $CsLnHgSe_3$ (Ln = La, Ce, Pr, Nd, Sm, Gd, Y) have been synthesized at 1123 K. These isostructural materials crystallize in the layered $KZrCuS_3$ structure type in the orthorhombic space group *Cmcm* and are group *X* extensions of the previously characterized Zn compounds. The structure is composed of two-dimensional $^2_\infty[LnMSe_3]$ layers that stack perpendicular to [010] and are separated by layers of face- and edge-sharing $CsSe_8$ bicapped trigonal prisms. Because there are no Se–Se bonds in the structure of $CsLnMSe_3$ (M = Zn, Cd, Hg), the formal oxidation states of Cs/Ln/M/Se are 1+/3+/2+/2–. $CsSmHgSe_3$ does not adhere to the Curie–Weiss law, whereas $CsCeHgSe_3$ and $CsGdHgSe_3$ are Curie–Weiss paramagnets with μ_{eff} values of 2.77 and 7.90 μ_B, corresponding well with the theoretical values of 2.54 and 7.94 μ_B for Ce^{3+} and Gd^{3+}, respectively. Single-crystal optical absorption measurements were performed with polarized light perpendicular to the (010) and (001) crystal faces of these materials. The band gaps of the (010) crystal faces range from 1.94 eV ($CsCeHgSe_3$) to 2.58 eV ($CsYCdSe_3$) whereas those of the (001) crystal faces span the range 2.37 eV ($CsSmHgSe_3$) to 2.54 eV ($CsYCdSe_3$ and $CsYHgSe_3$). The largest band gap variation between crystal faces is 0.06 eV for $CsYCdSe_3$. Theoretical calculations for $CsYMSe_3$ indicate that these materials are direct band gap semiconductors whose colors and optical band gaps are dependent upon the orbitals of Y, M, and Se.

Introduction

Compounds that contain a combination of d- and f-elements are of great interest in solid-state chemistry owing to their varied physical properties, which include superconductivity,[1] heavy fermion behavior,[2,3] and rare-earth−transition-metal exchange interactions.[4] A subgroup of these compounds encompasses the 3d−4f chalcogenides.[5] These show varied stoichiometries and structures and presumably varied physical properties, although the latter have been minimally investigated. Studies of these chalcogenides have focused on the ternary compounds, with the "misfit structures" ($[LnQ]_xMQ_2$)[6] and spinel phases (Ln_2MQ_4)[7−9] investigated the most extensively. However, the study of quaternary chalcogenide systems has increased over recent years primarily because of the use of the reactive flux method.[10] The d-element in these quaternary systems has been predominantly a magnetically silent coinage metal; moreover, the compounds undergo no long-range magnetic transitions, and reported optical data are scarce.

However, the investigation of the optical properties, i.e., absorption and luminescence, of materials is a significant aspect of solid-state chemistry, particularly of chalcogenides, owing to the industrial importance of the binary MSe (M = Zn, Cd, Hg) semiconductors. Numerous studies have been conducted on these binary compounds, and some under-

* To whom correspondence should be addressed. E-mail: ibers@chem.northwestern.edu.

(1) Fischer, O. *Springer Ser. Solid-State Sci.* **1990**, *90*, 96−112.
(2) Raymond, S.; Rueff, J. P.; Shapiro, S. M.; Wochner, P.; Sette, F.; Lejay, P. *Solid State Commun.* **2001**, *118*, 473−477.
(3) Goldman, A. I.; Stassis, C.; Canfield, P. C.; Zaretsky, J.; Dervenagas, P.; Cho, B. K.; Johnston, D. C.; Sternlieb, B. *Phys. Rev. B* **1994**, *50*, 9668−9671.
(4) Herbst, J. F. *Rev. Mod. Phys.* **1991**, *63*, 819−898.
(5) Mitchell, K.; Ibers, J. A. *Chem. Rev.* **2002**, *102*, 1929−1952.
(6) Rouxel, J.; Meerschaut, A.; Wiegers, G. A. *J. Alloys Compd.* **1995**, *229*, 144−157.
(7) Range, K.-J.; Eglmeier, C. *J. Alloys Compd.* **1991**, *176*, L13−L16.
(8) Ben-Dor, L.; Shilo, I.; Felner, I. *J. Solid State Chem.* **1979**, *28*, 363−367.
(9) Tomas, A.; Brossard, L.; Guittard, M. *J. Solid State Chem.* **1980**, *34*, 11−16.
(10) Sunshine, S. A.; Kang, D.; Ibers, J. A. *J. Am. Chem. Soc.* **1987**, *109*, 6202−6204.

10.1021/ic020733f CCC: $25.00
Published on Web 06/05/2003

Table 1. $CsLnMSe_3$ Compounds Synthesized[a] and Structurally Characterized

	La	Ce	Pr	Nd	Pm	Sm	Eu	Gd	Tb	Dy	Y	Ho	Er	Tm	Yb
Zn[b]						X[c]		X	X	X	X	X	X	X	X
Cd	∇[d]	X	X	∇		X		X	X	X	X				
Hg	X	X	X	X		X		X	∇	∇	X				

[a] Except for Pm, a blank indicates that the attempted synthesis was unsuccessful. [b] Information on $CsLnZnSe_3$ compounds was taken from ref 15. [c] An X indicates the compound was characterized using single-crystal X-ray diffraction techniques. [d] A ∇ indicates the compound was characterized using EDX measurements only.

standing of the relationship between their structural and physical properties has been gained.[11] Unfortunately, such understanding of the more complex ternary and quaternary chalcogenides is lacking.

It is well documented that MSe semiconductors may be doped with d- or f-metal cations that act as activators to modify the luminescent and magnetic properties of the parent material.[12,13] We have applied this principle to the two-dimensional $KZrCuS_3$ structure type and produced the isostructural $CsLnZnSe_3$ compounds that exhibit interesting variations of the optical properties of ZnSe and show the magnetic properties of the Ln^{3+} cations.[14,15] We demonstrated that the optical band gaps of the $CsLnZnSe_3$ compounds and accordingly their colors are dependent on crystal orientation and chemical composition. Here we extend this research to additional members of the $CsLnMSe_3$ (M = Cd, Ln = Ce, Pr, Sm, Gd, Tb, Dy, Y; M = Hg, Ln = La, Ce, Pr, Nd, Sm, Gd, Y) family. We also present the results of theoretical calculations that indicate which factors have the greatest effect on the optical properties of these compounds.

For convenience, in Table 1 we tabulate those $CsLnMSe_3$ compounds (M = Zn, Cd, Hg) whose crystal structures we have determined.

Experimental Section

Syntheses. The following reagents were used as obtained: Cs (Aldrich, 99.5%), La (Cerac, 99.9%), Ce (Alfa Aesar, 99.9%), Pr (Strem, 99.9%), Nd (Cerac, 99.9%), Sm (Alfa Aesar, 99.9%), Gd (Strem, 99.9%), Tb (Alfa Aesar, 99.9%), Dy (Alfa Aesar, 99.9%), Yb (Strem, 99.9%), Y (Alfa Aesar, 99.9%), Zn (Johnson Matthey, 99.99%), Cd (Alfa Aesar, 99.5%), HgSe (Strem, 99.99%), Se (Cerac, 99.99%), and CsI (Aldrich, 99.99%). Cs_2Se_3, the reactive flux[10] employed in the syntheses, was prepared by the stoichiometric reaction of the elements in liquid NH_3. Reaction mixtures were loaded into carbon-coated fused-silica tubes in an Ar filled glovebox. These tubes were sealed under a 10^{-4} Torr atmosphere and then placed in a computer-controlled furnace. The products of these reactions, as determined by the examination of selected single crystals with an EDX-equipped Hitachi S-3500 SEM, were consistent with the stated compositions. Several of the $CsLnMSe_3$ compounds are air sensitive, exhibiting signs of surface decomposition after being exposed to the atmosphere for several hours.

$CsLnZnSe_3$. The syntheses of $CsLnZnSe_3$ were detailed earlier.[15]

$CsLnCdSe_3$ and $CsLnHgSe_3$. These compounds (Table 1) were prepared in a manner similar to that employed in the preparation of the $CsLnZnSe_3$ compounds. The Cd compounds employed mixtures of 0.3 mmol of Cs_2Se_3, 0.5 of mmol Ln, 0.5 mmol of Cd, 1.0 mmol of Se, and approximately 150 mg of CsI; the Hg compounds employed 0.3 mmol of Cs_2Se_3, 0.5 of mmol Ln, 0.5 mmol of HgSe, 0.5 mmol of Se, and approximately 150 mg of CsI. The samples were heated to 1123 K in 24 h, kept at 1123 K for 96 h, and cooled to 473 K in 96 h, and then the furnace was turned off. The reaction mixtures were washed with water and then *N*,*N*-dimethylformamide and finally dried with acetone. Transparent, colored needles and plates of $CsLnMSe_3$ were obtained. $CsPrCdSe_3$, $CsDyCdSe_3$, $CsPrHgSe_3$, and $CsNdHgSe_3$ were obtained in very low yields (<10%) whereas the remaining compounds were synthesized in 85−100% yields (based upon Ln). In those instances of low yields, the desired product is contaminated with an unidentified ternary phase (Cs/Ln/Se).

Structure Determinations. Structural data for $CsLnZnSe_3$ were reported previously.[15] For the present $CsLnMSe_3$ (M = Cd, Hg) compounds detailed in Table 1, single-crystal X-ray diffraction data were collected with the use of graphite-monochromatized Mo Kα radiation ($\lambda = 0.71073$ Å) at 153 K on a Bruker Smart-1000 CCD diffractometer.[16] The crystal-to-detector distance was 5.023 cm. Crystal decay was monitored by recollecting 50 initial frames at the end of data collection. Data were collected by a scan of 0.3° in ω in groups of 606, 606, 606, and 606 frames at φ settings of 0°, 90°, 180°, and 270° for $CsLnCdSe_3$ (Ln = Sm, Gd, Tb, Dy, Y) and $CsLnHgSe_3$ (Ln = La, Pr, Nd, Sm, Gd, Y), and in groups of 606, 606, and 606 frames at φ settings of 0°, 120°, and 240° for $CsCeCdSe_3$, $CsPrCdSe_3$, and $CsCeHgSe_3$. The exposure times varied from 10 to 15 s/frame. The collection of the intensity data was carried out with the program SMART.[16] Cell refinement and data reduction were carried out with the use of the program SAINT,[16] and face-indexed absorption corrections were performed numerically with the use of the program XPREP.[17] Then the program SADABS[16] was employed to make incident beam and decay corrections.

The structures were solved with the direct methods program SHELXS and refined with the full-matrix least-squares program SHELXL of the SHELXTL suite of programs.[17] Each final refinement included anisotropic displacement parameters and a secondary extinction correction. Additional experimental details are shown in Tables 2 and 3. Tables 4 and 5 present selected bond distances.

Magnetic Susceptibility Measurements. Measurements on $CsCeHgSe_3$ (31.0 mg), $CsSmHgSe_3$ (35.3 mg), and $CsGdHgSe_3$ (56.4 mg) were carried out with the use of a Quantum Design SQUID magnetometer (MPMS5 Quantum Design). Magnetic measurements were not performed on $CsPrHgSe_3$ or $CsNdHgSe_3$ because these compounds were obtained in low yields. The composition of each sample was verified by EDX measurements. All samples were ground and loaded into gelatin capsules. Zero-field cooled (ZFC) susceptibility data were collected between 5 and 300 K for $CsCeHgSe_3$ and $CsGdHgSe_3$ whereas for $CsSmHgSe_3$ data were collected between 5 and 200 K at an applied field of

(11) Solymar, L.; Walsh, D. *Electrical Properties of Materials*, 6th ed.; Oxford University Press: New York, 1998.
(12) West, A. R. *Solid State Chemistry and its Applications*; John Wiley & Sons: New York, 1984.
(13) Hommel, D.; Busse, W.; Gumlich, H.-E.; Suisky, D.; Röseler, J.; Swiatek, K.; Godlewski, M. *J. Cryst. Growth* **1990**, *101*, 393−403.
(14) Huang, F. Q.; Mitchell, K.; Ibers, J. A. *Inorg. Chem.* **2001**, *40*, 5123−5126.
(15) Mitchell, K.; Haynes, C. L.; McFarland, A. D.; Van Duyne, R. P.; Ibers, J. A. *Inorg. Chem.* **2002**, *41*, 1199−1204.
(16) *SMART Version 5.054 Data Collection and SAINT-Plus Version 6.22 Data Processing Software for the SMART System*; Bruker Analytical X-ray Instruments, Inc.: Madison, WI, 2000.
(17) Sheldrick, G. M. *SHELXTL DOS/Windows/NT Version 6.12*; Bruker Analytical X-ray Instruments, Inc.: Madison, WI, 2000.

Table 2. Crystal Data and Structure Refinements for $CsLnCdSe_3$[a]

	$CsCeCdSe_3$	$CsPrCdSe_3$	$CsSmCdSe_3$	$CsGdCdSe_3$	$CsTbCdSe_3$	$CsDyCdSe_3$	$CsYCdSe_3$
fw	622.31	623.10	632.54	639.44	641.11	644.69	571.10
a, Å	4.3883(5)	4.3556(9)	4.2995(4)	4.2784(4)	4.2612(3)	4.2419(3)	4.2386(5)
b, Å	15.7576(18)	15.747(3)	15.7793(15)	15.8322(15)	15.8319(12)	15.8274(12)	15.819(2)
c, Å	11.4236(13)	11.348(3)	11.2010(10)	11.1548(11)	11.1096(9)	11.0828(8)	11.0639(14)
V, Å^3	789.93(16)	778.3(3)	759.91(12)	755.59(13)	749.49(10)	744.08(9)	741.82(16)
ρ_c, g cm^{-3}	5.233	5.318	5.529	5.621	5.682	5.755	5.114
μ, cm^{-1}	266.30	274.40	294.19	305.93	314.30	321.95	300.83
$R(F)$[b]	0.0171	0.0235	0.0199	0.0245	0.0186	0.0191	0.0195
$R_w(F^2)$[c]	0.0417	0.0597	0.0536	0.0648	0.0516	0.0560	0.0477

[a] For all structures, $Z = 4$, space group = *Cmcm*, $T = 153(2)$ K, and $\lambda = 0.71073$ Å. [b] $R(F) = \sum||F_o| - |F_c||/\sum|F_o|$ for $F_o^2 > 2\sigma(F_o^2)$. [c] $R_w(F^2) = \{\sum[w(F_o^2 - F_c^2)^2]/\sum wF_o^4\}^{1/2}$ for all data. $w^{-1} = \sigma^2(F_o^2) + (q \times F_o^2)^2$ for $F_o^2 \geq 0$ and $w^{-1} = \sigma^2(F_o^2)$ for $F_o^2 < 0$. $q = 0.025$ for Ln = Ce; $q = 0.03$ for Ln = Y; and $q = 0.04$ for the others.

Table 3. Crystal Data and Structure Refinements for $CsLnHgSe_3$[a]

	$CsLaHgSe_3$	$CsCeHgSe_3$	$CsPrHgSe_3$	$CsNdHgSe_3$	$CsSmHgSe_3$	$CsGdHgSe_3$	$CsYHgSe_3$
fw	709.29	710.50	711.29	714.62	720.73	727.63	659.29
a, Å	4.4002(4)	4.3719(5)	4.3386(4)	4.3202(3)	4.294(2)	4.2763(14)	4.2226(18)
b, Å	15.7279(14)	15.7658(17)	15.7404(15)	15.7771(11)	15.878(6)	15.877(5)	15.839(7)
c, Å	11.4052(10)	11.3166(12)	11.2441(10)	11.1981(8)	11.143(4)	11.114(4)	10.997(5)
V, Å^3	789.31(12)	780.01(15)	767.87(12)	763.27(9)	759.8(5)	754.6(4)	735.5(5)
ρ_c, g cm^{-3}	5.969	6.050	6.153	6.219	6.301	6.405	5.954
μ, cm^{-1}	430.30	439.02	450.13	457.04	468.07	481.38	483.00
$R(F)$[b]	0.0192	0.0243	0.0219	0.0207	0.0225	0.0187	0.0225
$R_w(F^2)$[c]	0.0473	0.0560	0.0558	0.0492	0.0543	0.0465	0.0564

[a] For all structures, $Z = 4$, space group = *Cmcm*, $T = 153(2)$ K, and $\lambda = 0.71073$ Å. [b] $R(F) = \sum||F_o| - |F_c||/\sum|F_o|$ for $F_o^2 > 2\sigma(F_o^2)$. [c] $R_w(F^2) = \{\sum[w(F_o^2 - F_c^2)^2]/\sum wF_o^4\}^{1/2}$ for all data. $w^{-1} = \sigma^2(F_o^2) + (q \times F_o^2)^2$ for $F_o^2 \geq 0$ and $w^{-1} = \sigma^2(F_o^2)$ for $F_o^2 < 0$. $q = 0.03$ for Ln = La, Ce, Nd, Gd, and Y; and $q = 0.04$ for the others.

Table 4. Selected Bond Lengths (Å) for $CsLnCdSe_3$

	$CsCeCdSe_3$	$CsPrCdSe_3$	$CsSmCdSe_3$	$CsGdCdSe_3$	$CsTbCdSe_3$	$CsDyCdSe_3$	$CsYCdSe_3$
Cs−Se1 ×4	3.7850(5)	3.7787(8)	3.7803(5)	3.7888(7)	3.7899(5)	3.7894(5)	3.7875(6)
Cs−Se1 ×2	3.9385(6)	3.912(1)	3.8512(6)	3.8277(8)	3.8123(6)	3.8034(6)	3.7925(7)
Cs−Se2 ×2	3.6074(6)	3.596(1)	3.5891(7)	3.598(1)	3.5927(8)	3.5881(8)	3.5899(7)
Ln−Se1 ×4	2.9970(4)	2.9736(6)	2.9343(4)	2.9232(5)	2.9073(4)	2.8931(4)	2.8924(4)
Ln−Se2 ×2	3.0105(4)	2.9928(7)	2.9577(3)	2.9440(4)	2.9345(3)	2.9277(3)	2.9203(4)
Cd−Se1 ×2	2.6016(5)	2.5959(8)	2.5909(5)	2.5907(8)	2.5895(6)	2.5864(6)	2.5815(6)
Cd−Se2 ×2	2.7066(5)	2.6919(8)	2.6768(5)	2.6738(7)	2.6682(5)	2.6603(5)	2.6593(6)

Table 5. Selected Bond Lengths (Å) for $CsLnHgSe_3$

	$CsLaHgSe_3$	$CsCeHgSe_3$	$CsPrHgSe_3$	$CsNdHgSe_3$	$CsSmHgSe_3$	$CsGdHgSe_3$	$CsYHgSe_3$
Cs−Se1 ×4	3.7618(6)	3.7659(9)	3.7589(7)	3.7632(6)	3.786(1)	3.7845(9)	3.777(1)
Cs−Se1 ×2	3.9040(7)	3.873(1)	3.8454(8)	3.8263(6)	3.809(1)	3.787(1)	3.745(2)
Cs−Se2 ×2	3.5937(9)	3.594(1)	3.584(1)	3.5862(9)	3.605(1)	3.604(1)	3.593(2)
Ln−Se1 ×4	3.0264(4)	3.0025(6)	2.9777(5)	2.9663(4)	2.9441(9)	2.9348(8)	2.894(1)
Ln−Se2 ×2	3.0128(4)	2.9933(5)	2.9751(4)	2.9642(3)	2.948(1)	2.9412(9)	2.909(1)
Hg−Se1 ×2	2.5971(6)	2.5964(9)	2.5915(7)	2.5906(6)	2.587(1)	2.5940(9)	2.577(1)
Hg−Se2 ×2	2.7610(6)	2.7528(8)	2.7361(7)	2.7345(6)	2.731(1)	2.7290(9)	2.710(1)

500 G. All measurements were corrected for core diamagnetism.[18] The susceptibility data in the temperature range 100−300 K were fit by a least-squares method to the Curie−Weiss equation $\chi = C/(T - \theta_p)$, where C is the Curie constant and θ_p is the Weiss constant. The effective magnetic moment (μ_{eff}) was calculated from the equation $\mu_{eff} = (7.997C)^{1/2}\mu_B$.[19] Magnetic measurements were not performed on the $CsLnCdSe_3$ compounds owing to their contamination with unidentified Cs/Ln/Se phases.

Optical Measurements. Absorption measurements were performed on $CsYbZnSe_3$, $CsLnCdSe_3$ (Ln = Ce, Sm, Gd, Tb, Dy, Y), and $CsLnHgSe_3$ (Ln = La, Ce, Sm, Gd, Y) single crystals with the use of an Ocean Optics model S2000 spectrometer over the range 400 nm (3.10 eV) to 800 nm (1.55 eV) at 293 K. The apparatus employed in the measurements reported here improves upon that used previously[15] by simplifying the alignment procedure and increasing the collection efficiency. The spectrometer was fiber optically coupled to a Nikon TE300 inverted microscope. White light originated from the TE300 lamp and passed through a polarizer before reaching the sample. Face-indexed single crystals with typical dimensions of 300, 20, and 50 μm in the [100], [010], and [001] directions, respectively, were positioned at the focal point above the 20× objective with the use of a goniometer mounted on translation stages (Line Tool Company). The light transmitted through the crystal was then spatially filtered before being focused into the 400 μm core diameter fiber coupled to the spectrometer. Fine alignment of the microscope assembly was achieved by maximizing the transmission of the lamp profile. The extinction spectra of both the (010) and (001) crystal planes (light perpendicular to the *ac* and *ab* crystal planes, respectively) were recorded.

(18) *Theory and Applications of Molecular Diamagnetism*; Mulay, L. N., Boudreaux, E. A., Eds.; Wiley-Interscience: New York, 1976.
(19) O'Connor, C. J. *Prog. Inorg. Chem.* **1982**, *29*, 203−283.

Table 6. Face-Dependent Optical Band Gaps for $CsLnMSe_3$ Materials

compd	color	(010) crystal face[a] (eV)	(001) crystal face[b] (eV)
$CsSmZnSe_3$[c]	bright yellow	2.63	2.43
$CsErZnSe_3$[c]	pale yellow	2.63	2.56
$CsYbZnSe_3$[d]	red	2.10	1.97
$CsYZnSe_3$[c]	pale yellow	2.41	2.29
$CsCeCdSe_3$	yellow	2.40	2.40
$CsSmCdSe_3$	yellow	2.47	2.45
$CsYCdSe_3$	yellow	2.48	2.54
$CsLaHgSe_3$	amber	2.51	2.46
$CsCeHgSe_3$	red	1.94	
$CsSmHgSe_3$	yellow	2.36	2.37
$CsYHgSe_3$	yellow	2.58	2.54

[a] Light in the [010] direction. [b] Light in the [001] direction. [c] Data from ref 15. [d] Values of 1.93 and 1.88 eV for (010) and (001), respectively, were determined earlier (ref 15) from a different sample preparation.

In order to account for incomplete filling of the probe spot size by some faces of the mounted single crystals the absorption data were scaled with the use of the following formula:[20]

$$\eta = (2/(\pi D^2))[w(D^2 - w^2)^{1/2} + D^2 \arcsin(w/D)] \quad (1)$$

where η is the fraction of the spot size filled by the crystal, w is the width of the crystal, and D is the white light probe diameter. The width was taken to be the separation of the (010) and $(0\bar{1}0)$ or (001) and $(00\bar{1})$ faces when the (010) and (001) faces were measured, respectively. The scaled absorption value and the crystal thickness were then used to calculated the molar absorption coefficient (α) of each single-crystal sample. The band gap for these crystals is a direct transition, and the data were manipulated accordingly. From α and the incident photon energy ($h\nu$), the direct band gap (E_g) for these semiconductors[21] was calculated according to the following relation:

$$(\alpha h\nu)^2 \sim h\nu - E_g \quad (2)$$

E_g was calculated in the following manner: (1) $(\alpha h\nu)^2$ was plotted versus $h\nu$; (2) a line was fit to the spectral baseline for energies slightly lower than the absorption edge; (3) a line was fit to the most linear region of the absorption edge; and (4) the photon energy of the intersection of these two lines defines the reported band gap energies. These measurements and linear regression calculations were carried out for both the (010) and (001) faces of those materials listed in Table 6. In that table, we also list previous results for such calculations on some $CsLnZnSe_3$ compounds.[15]

Owing to problems with baseline curvature, the linear regression method described here could not be applied to the analysis of the present optical data from $CsLnCdSe_3$ (Ln = Pr, Gd, Tb, Dy) and $CsLnHgSe_3$ (Ln = Pr, Nd, Gd) and for the earlier optical data for $CsLnZnSe_3$ (Ln = Tb, Dy, Ho, Tm).[15] Therefore, an alternative data analysis technique, a simple inflection-point analysis, was employed. In this method, the optical band gap is taken to be the value of the energy E where $\partial^2 A/\partial E^2 = 0$, where A is the absorbance. Utilization of this analysis technique minimizes the influence of air sensitivity (manifested as baseline curvature) and does not require thickness or fill factor corrections. Although this method slightly overestimates the location of the band edge (see details later in this text), it is reproducible, it is independent of the spectral baseline, and it provides useful information for spectra with poor signal-to-noise ratios. This treatment of the data leads to a precision of ± 0.01 eV, as deduced from measurements on several crystals of the same composition and synthesis.

Theoretical Calculations. The calculations for the $CsYMSe_3$ (M = Zn, Cd, Hg) compounds were performed with the linearized augmented plane-wave ((L)APW) + local orbitals (lo) method with the use of the WIEN2k program package.[22] The exchange-correlation functional was taken within the local density approximation (LDA).[23] The muffin-tin radii were chosen to be 2.6 au for Cs, 2.4 au for Y, and 2.3 au for M (M = Zn, Cd, Hg) and Se. The plane-wave expansion cutoffs were 7 au^{-1} for expanding the wave function (RKMAX) and 14 au^{-1} for expanding the densities and potentials (GMAX). All relativistic effects were taken into account. Brillouin-zone integrations within the self-consistency cycles were performed by means of the tetrahedron method[24] with 40 inequivalent k points corresponding to 192 k points throughout the Brillouin zone for $CsYMSe_3$. The density-of-states (DOS) was also calculated with the modified tetrahedron method.

Results

Syntheses. The $CsLnZnSe_3$ materials were not obtained with the lighter (and hence larger) rare-earth elements (Ln = La−Nd), whereas the $CsLnHgSe_3$ compounds were not obtained with the heavier rare-earth elements (Ln = Er−Yb). It is clear from Table 1 that as the atomic radius of the transition-metal increases in the $CsLnMSe_3$ compounds so does the radius of the rare-earth, presumably to maintain the anionic framework of edge-sharing MSe_4 tetrahedra and $LnSe_6$ octahedra and hence the stability of the structure. Generally, the yields of compounds detailed in Table 1 were 85−100%; for unknown reasons, the reactions involving Pr and Nd had yields of 10% or less. A few compounds, namely $CsNdCdSe_3$, $CsTbHgSe_3$, and $CsDyHgSe_3$, were synthesized in very low yields, and the crystals obtained were unsuitable for single-crystal X-ray diffraction studies. No Eu compounds could be synthesized, presumably because of the propensity of Eu to be formally 2+, rather than 3+, in chalcogenide systems, examples being $EuZrS_3$,[25] $EuZrSe_3$,[26] and $EuCr_2Te_4$.[27]

Preliminary EDX measurements indicate that the $CsLnMSe_3$ series may be extended to include S and Te analogues and to $CsLnMnSe_3$ compounds.

Structure. The structure of the isostructural $CsLnMSe_3$ compounds, which is of the $KZrCuS_3$ structure type, is illustrated in Figure 1. It is composed of two-dimensional $^2_\infty[LnMSe_3]$ layers that stack perpendicular to [010] and are separated by Cs atoms. The Cs atoms are coordinated to eight Se atoms in a bicapped trigonal prismatic arrangement. Each $CsSe_8$ prism has two face-sharing neighbors (labeled 1a and

(20) Altkorn, R.; Malinsky, M. D.; Van Duyne, R. P.; Koev, I. *Appl. Spectrosc.* **2001**, *55*, 373−381.
(21) Bang, T.-H.; Choe, S.-H.; Park, B.-N.; Jin, M.-S.; Kim, W.-T. *Semicond. Sci. Technol.* **1996**, *11*, 1159−1162.
(22) Blaha, P.; Schwarz, K.; Madsen, G.; Kvasnicka, D.; Luitz, J. *WIEN2k*; Vienna University of Technology, 2001.
(23) Perdew, J. P.; Wang, Y. *Phys. Rev. B: Condens. Matter* **1992**, *45*, 13244−13249.
(24) Blöchl, P. E.; Jepsen, O.; Andersen, O. K. *Phys. Rev. B: Condens. Matter* **1994**, *49*, 16223−16233.
(25) Kazarbina, T. V.; Maksimov, Y. M.; Serebrennikov, V. V. *Russ. J. Inorg. Chem. (Transl. of Zh. Neorg. Khim.)* **1981**, *26*, 1073−1074.
(26) Mar, A.; Ibers, J. A. *Acta Crystallogr., Sect. C: Cryst. Struct. Commun.* **1992**, *48*, 771−773.
(27) Shirinov, K. L.; Aliev, O. M. *Inorg. Mater. (Transl. of Neorg. Mater.)* **1988**, *24*, 948−951.

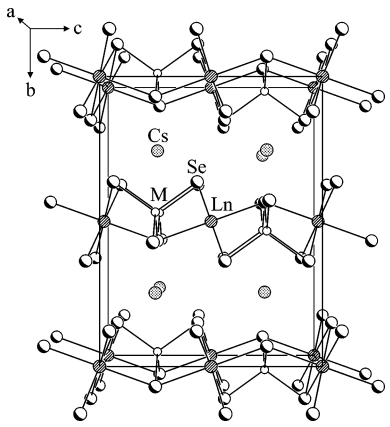

Figure 1. Unit cell of $CsLnMSe_3$ viewed down [100].

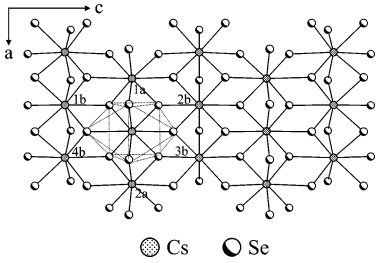

Figure 2. $^2_\infty[CsSe_3]$ layer viewed down [010].

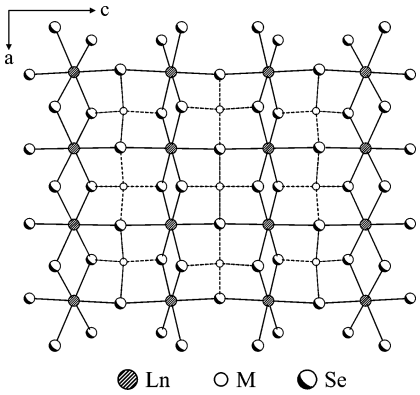

Figure 3. $^2_\infty[LnMSe_3]$ layer viewed down [010].

2a) along [100] and four edge-sharing ones (labeled 1b to 4b) along [001] to form a $^2_\infty[CsSe_3]$ layer (Figure 2). The Ln atoms are coordinated to a slightly distorted octahedron of six Se atoms, whereas the M atoms are coordinated to a distorted tetrahedron of four Se atoms. The $^2_\infty[LnMSe_3]$ layer is constructed from these $LnSe_6$ octahedra and MSe_4 tetrahedra, as shown in Figure 3. Each $LnSe_6$ octahedron shares its edges with two other octahedra along [100] to form a one-dimensional $^1_\infty[LnSe_4]$ chain. The MSe_4 tetrahedra form one-dimensional $^1_\infty[MSe_3]$ chains along [100] by sharing vertices with two neighboring tetrahedra. Each tetrahedron in the $^1_\infty[MSe_3]$ chain links with four $LnSe_6$ octahedra by edge-sharing along [001] to form the $^2_\infty[LnMSe_3]$ layers.

Because there are no Se−Se bonds in the structure of $CsLnMSe_3$, the formal oxidation states of Cs/Ln/M/Se are 1+/3+/2+/2−. Several other isostructural compounds are known with the oxidation states A/Ln/M/Q of 1+ or 2+/3+ or 4+/1+/2−, such as the parent $KZrCuQ_3$ (Q = S, Se, Te),[28] $CsUCuTe_3$,[29] $KUCuSe_3$,[30] $CsCeCuS_3$,[30] $TlZrCuTe_3$,[31] and $BaLnCuQ_3$.[32−34] However, to the best of our knowledge the present $CsLnHgSe_3$ compounds are the only known examples of d−f quaternary mercury chalcogenides. Other quaternary mercury chalcogenides include $KSbHgS_3$,[35] $RbSbHgSe_3$,[36] $RbSbHgTe_3$,[37] and $CsSbHgSe_3$.[36] $RbSbHgSe_3$, $RbSbHgTe_3$, and $CsSbHgSe_3$ have a structure that is closely related to the present one, but Sb^{3+} occupies the Wyckoff 8f site with an occupancy of 0.5 rather than the 4a site for Ln^{3+} in $CsLnMSe_3$. $KSbHgS_3$ adopts an entirely different one-dimensional structure that contains $[SbS_3]^{3-}$ pyramidal units and Hg atoms coordinated in a linear fashion.

In the present materials, all of the bond lengths are normal (Tables 4 and 5). Those involving Ln reflect the lanthanide contraction. The ranges of bond lengths are consistent, for example, with those of 2.940(2)−3.019(2) Å for La−Se in β-$BaLaCuSe_3$;[33] 3.018(2)−3.158(2) Å for Ce−Se in KCe_2CuSe_6;[38] 2.911(2)−3.079(2) Å for Pr−Se in Pr_3InSe_6;[39] 2.902(3)−2.949(3) Å for Nd−Se in $Ba_4Nd_2Cd_3Se_{10}$;[40] 2.8595(4)−3.0086(3) Å for Sm−Se in $CsSm_2CuSe_4$;[41] 2.8871(1)−2.928(1) Å for Gd−Se in $BaGdAuSe_3$;[42] 2.8509(6)−2.9240(6) Å for Tb−Se in $CsTb_2Ag_3Se_5$;[41] 2.822(1)−2.9385(8) Å for Dy−Se in $RbDy_2CuSe_4$;[43] 2.879(1)−2.910(1) Å for Y−Se in $BaYAgSe_3$;[34] 3.4281(8)−3.9527(3) Å for Cs−Se in $CsSm_2CuSe_4$;[41] 2.544(4)−2.792(4) Å for Cd−Se in $Ba_4Nd_2Cd_3Se_{10}$;[40] and the Hg−Se distances of 2.608(2)−2.759(2) Å in $RbHgSbSe_3$.[36]

Magnetic Properties. Plots of the reciprocal of the molar susceptibility ($1/\chi$) versus T for $CsCeHgSe_3$, $CsSmHgSe_3$, and $CsGdHgSe_3$ are shown in Figure 4. $CsGdHgSe_3$ exhibits Curie−Weiss paramagnetism over the temperature range 5−300 K with values of $C = 7.80(1)$ emu K mol^{-1} and $\theta_p = -2.63(5)$ K, and a calculated effective magnetic moment for Gd^{3+} of 7.90 μ_B in good agreement with the theoretical value of 7.94 μ_B.[44] As is typical of Sm^{3+} chalcogenides, i.e., Sm_3MSe_6 (M = In, Cr)[45] and $CsSmZnSe_3$,[15] the magnetic data for $CsSmHgSe_3$ do not follow the Curie−Weiss law

(28) Mansuetto, M. F.; Keane, P. M.; Ibers, J. A. *J. Solid State Chem.* **1992**, *101*, 257−264.
(29) Cody, J. A.; Ibers, J. A. *Inorg. Chem.* **1995**, *34*, 3165−3172.
(30) Sutorik, A. C.; Albritton-Thomas, J.; Hogan, T.; Kannewurf, C. R.; Kanatzidis, M. G. *Chem. Mater.* **1996**, *8*, 751−761.
(31) Pell, M. A.; Ibers, J. A. *J. Alloys Compd.* **1996**, *240*, 37−41.
(32) Huang, F. Q.; Choe, W.; Lee, S.; Chu, J. S. *Chem. Mater.* **1998**, *10*, 1320−1326.
(33) Christuk, A. E.; Wu, P.; Ibers, J. A. *J. Solid State Chem.* **1994**, *110*, 330−336.
(34) Wu, P.; Christuk, A. E.; Ibers, J. A. *J. Solid State Chem.* **1994**, *110*, 337−344.
(35) Imafuku, M.; Nakai, I.; Nagashima, K. *Mater. Res. Bull.* **1986**, *21*, 493−501.
(36) Chen, Z.; Wang, R.-J.; Li, J. *Mater. Res. Soc. Symp. Proc.* **1999**, *547*, 419−424.
(37) Li, J.; Chen, Z.; Wang, X.; Proserpio, D. M. *J. Alloys Compd.* **1997**, *262*−*263*, 28−33.
(38) Klawitter, Y.; Näther, C.; Jess, I.; Bensch, W.; Kanatzidis, M. G. *Solid State Sci.* **1999**, *1*, 421−431.
(39) Aleandri, L. E.; Ibers, J. A. *J. Solid State Chem.* **1989**, *79*, 107−111.
(40) Yang, Y.; Ibers, J. A. *J. Solid State Chem.* **2000**, *149*, 384−390.
(41) Huang, F. Q.; Ibers, J. A. *J. Solid State Chem.* **2001**, *158*, 299−306.
(42) Yang, Y.; Ibers, J. A. *J. Solid State Chem.* **1999**, *147*, 366−371.
(43) Huang, F. Q.; Ibers, J. A. *J. Solid State Chem.* **2000**, *151*, 317−322.
(44) Kittel, C. *Introduction to Solid State Physics*, 6th ed.; Wiley: New York, 1986.
(45) Tougait, O.; Ibers, J. A. *Inorg. Chem.* **2000**, *39*, 1790−1794.

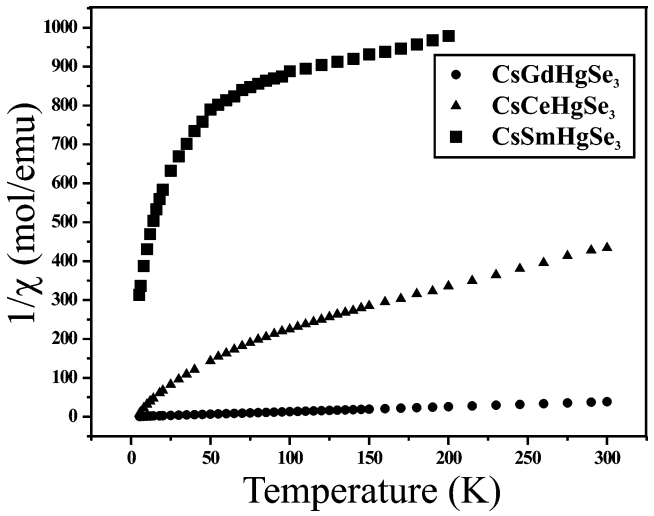

Figure 4. Inverse magnetic susceptibility ($1/\chi$) vs T for $CsCeHgSe_3$, $CsSmHgSe_3$, and $CsGdHgSe_3$.

because the effective moment of the 4f electrons has a temperature dependence that arises from low-lying multiplets.[46] And as is typical for Ce^{3+} chalcogenides, including $CsCeCuS_3$,[30] ACe_2CuQ_6 (A = K, Cs; Q = S, Se),[30] $TlCeQ_2$ (Q = Se, Te),[47] $NaCeS_2$,[48] and $BaCeCuQ_3$ (Q = S, Se),[34] the magnetic data for $CsCeHgSe_3$ deviate from the Curie−Weiss law below 100 K. Such deviations have been attributed to the crystal-field splitting of the $^2F_{5/2}$ ground state of Ce^{3+}.[48] However, above 100 K the molar susceptibility data for $CsCeHgSe_3$ adhere to the Curie−Weiss law and yield values of $C = 0.96(1)$ emu K mol^{-1}, $\theta_p = -120(2)$ K, and $\mu_{eff} = 2.77(3)\ \mu_B$, in reasonable agreement with the theoretical value of 2.54 μ_B for Ce^{3+}.[44] The large negative Weiss constant is indicative of a substantial degree of local antiferromagnetic coupling.

Absorption Spectra. A summary of the single-crystal absorption measurements calculated by means of the linear regression analysis for the present compounds and for the earlier $CsLnZnSe_3$ compounds[15] is presented in Table 6. The colors of these materials are consistent with the derived band gaps. The optical band gaps for the $CsLnCdSe_3$ compounds range from 2.40 to 2.48 eV for the (010) crystal face and from 2.40 to 2.54 eV for the (001) crystal face with $CsYCdSe_3$ exhibiting the largest face dependence (0.06 eV). The measured values for the $CsLnHgSe_3$ materials are similar and range from 1.94 to 2.58 eV for the (010) crystal face and from 2.37 to 2.54 eV for the (001) crystal face with $CsLaHgSe_3$ exhibiting the largest face dependence (0.05 eV). These differences are smaller than those observed earlier for the $CsLnZnSe_3$ compounds. Morever, there is no obvious correlation of the optical band gaps of the present $CsLnMSe_3$ materials with unit cell volume, as was noted earlier from the limited data on the $CsLnZnSe_3$ compounds.[15]

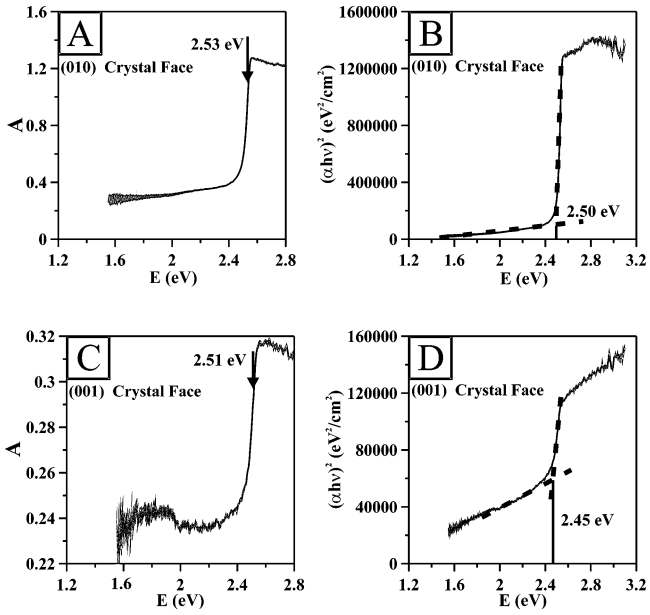

Figure 5. Optical absorption spectra for a $CsLaHgSe_3$ crystal and derivation of the band gaps by both the linear-regression and the inflection-point analyses. A and C show absorption spectra and inflection-point analysis of the (010) and (001) crystal faces, respectively. B and D show plots of $(\alpha h\nu)^2$ versus E and the determination of the band gaps by the linear-regression analysis for the (010) and (001) faces, respectively.

The optical band gaps of the compounds listed in Table 6 were compared with the values obtained by means of the inflection point method. Figure 5 displays the absorption spectra of $CsLaHgSe_3$ and the two methods used to derive the band gaps. We find that the inflection point method overestimates the location of the band edge by at least 0.2 eV and approximately 0.15 and 0.05 eV for the $CsLnZnSe_3$, $CsLnCdSe_3$, and $CsLnHgSe_3$ compounds, respectively. The lack of a consistent overestimation indicates that the shapes of the absorption curves differ among these compounds. Trends in the band gap values, as calculated by means of the inflection point analysis, did not differ significantly from those reported in Table 6. The optical band gaps, as obtained by the inflection point analysis, for $CsLnCdSe_3$ (Ln = Gd, Tb, Dy) and $CsGdHgSe_3$ are (compound, (010) crystal face, (001) crystal face, in eV) the following: $CsGdCdSe_3$, 2.60, 2.54; $CsTbCdSe_3$, 2.67, 2.60; $CsDyCdSe_3$, 2.57, 2.51; $CsGdHgSe_3$, 2.54, 2.53.

Single-crystal absorption measurements with both polarized and unpolarized light were carried out on a new sample of $CsYbZnSe_3$. There was no noticeable difference in the spectra obtained. Previous measurements on a different sample were made with unpolarized light. The optical band gaps calculated by means of the linear regression method for the (010) and (001) crystal faces are 2.10 and 1.97 eV, respectively, compared with values of 1.93 and 1.88 eV obtained previously.[15] The cause of these differences, which must lie with the samples, is unknown.

Theory. The band structures of $CsYZnSe_3$, $CsYCdSe_3$, and $CsYHgSe_3$ are very similar. The band structure of $CsYZnSe_3$ is displayed in Figure 6. The valence-band maxima and conduction-band minima are located at the Γ point; therefore, these compounds are direct gap semicon-

(46) Van Vleck, J. H. *The Theory of Electric and Magnetic Susceptibilities*; Oxford University Press: London, 1932.
(47) Duczmal, M.; Pawlak, L. *J. Magn. Magn. Mater.* **1988**, *76*−*77*, 195−196.
(48) Lueken, H.; Brüggemann, W.; Bronger, W.; Fleischhauer, J. *J. Less-Common Met.* **1979**, *65*, 79−88.

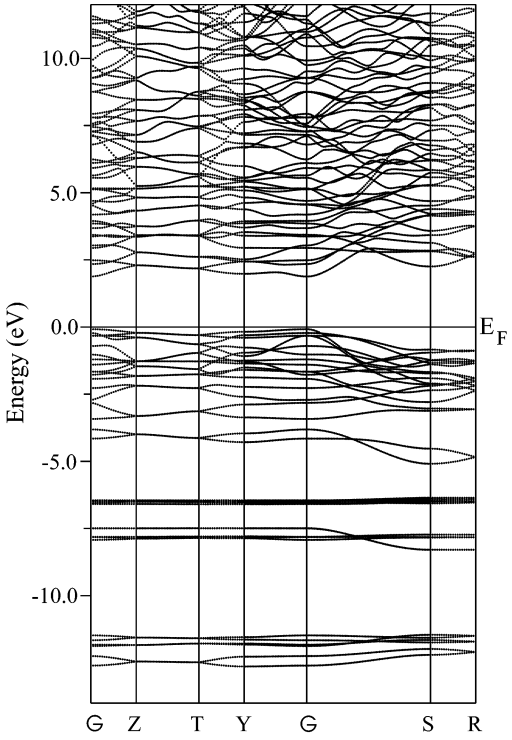

Figure 6. Band structure of $CsYZnSe_3$ where the special *k*-points in the figure are Γ (0,0,0), Y (0,1,0), Z (0,0,$^1/_2$), T (0,1,$^1/_2$), S ($^1/_2$,$^1/_2$,0), R ($^1/_2$,$^1/_2$,$^1/_2$).

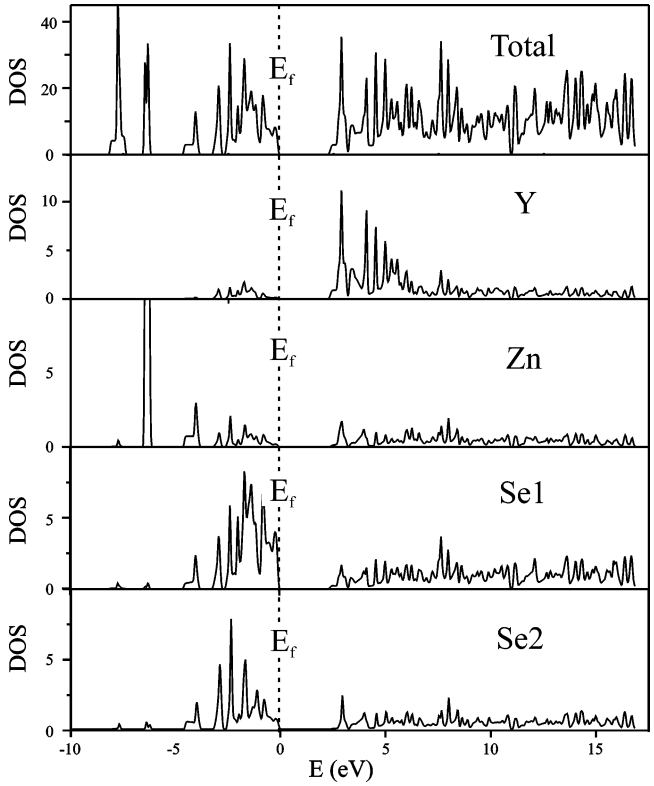

Figure 7. Total density-of-states and partial density-of-states (DOS) of $CsYZnSe_3$.

ductors. Although density functional theory is known to underestimate optical band gaps,[49,50] values of 2.11 and 2.16 eV were nevertheless obtained for $CsYZnSe_3$ and $CsYCdSe_3$, in surprisingly close agreement with the corresponding experimental values of 2.29[15] and 2.54 eV for the (001) crystal faces of $CsYZnSe_3$ and $CsYCdSe_3$, respectively. Presumably owing to computational difficulties caused by the heavy Hg atom, the agreement for the (001) crystal face of $CsYHgSe_3$ between the calculated band gap of 1.54 eV and the observed optical band gap of 2.54 eV is poorer. The overall covalence bands, especially near the Fermi surface, are not very disperse, an indication of limited orbital overlap. The dispersion along [010] is smaller than that along [100]. This finding is consistent with the crystal structure; in the [010] direction, the $^2_\infty[CsSe_3]$ layers limit the interactions of the $^2_\infty[LnMSe_3]$ layers that propagate along [100].

The band gaps of most of the $CsLnMSe_3$ (M = Zn, Cd, Hg) compounds are blue shifted relative to those of ZnSe, CdSe, and HgSe, whose band gaps are 2.58, 1.74, and −0.15 eV, respectively.[51] A similar shift was observed in the $A_2M_3Q_4$ (M = Cd, Hg)[52,53] and $A_2Hg_6Q_7$[53] compounds relative to the binaries and was attributed to the reduced dimensionality of these compounds in comparison with the three-dimensional MSe_4 tetrahedral network of MSe. Decreased dimensionality of these ternary phases was postulated to inhibit the orbital overlap of their $[M_xQ_y]^{n-}$ frameworks and lead to a narrowing of the electronic bands and a widening of the optical band gaps. This same argument may be applied to the $CsLnMSe_3$ compounds, in particular to M = Cd and Hg whose band gaps are significantly larger than those of CdSe and HgSe. The theoretical calculations indicate that the bonds that separate the covalently bonded $^1_\infty[MSe_3]$ chains from the $^1_\infty[LnSe_4]$ chains and the $^2_\infty[CsSe_3]$ layers are more ionic in nature than those in the MSe binaries. In effect, the dimensionality of the MSe_4 tetrahedral network in the $CsLnMSe_3$ compounds is reduced from that of the MSe binaries resulting in significant band gap widening. Whereas the band gaps of the (010) crystal faces of $CsSmZnSe_3$ and $CsErZnSe_3$ are blue shifted relative to that of ZnSe, those of $CsYbZnSe_3$ and $CsYZnSe_3$ are not. The $ZnSe_4$ tetrahedra of $CsSmZnSe_3$ and $CsErZnSe_3$ are slightly more distorted than those of $CsYbZnSe_3$ and $CsYZnSe_3$. This may influence the orbital overlap and the band gaps.

The total density-of-states and partial density-of-states (DOS) of $CsYZnSe_3$ are shown in Figure 7. LDA calculations of the density-of-states are very reliable and do not exhibit the errors found in band gap calculations. The calculations indicate that the highest occupied molecular orbitals (HOMOs) of $CsYZnSe_3$ are primarily Se1 (4p) and Se2 (4p) in character, whereas the lowest unoccupied molecular orbitals (LUMOs) have contributions from Zn (4s and 4p), Y (4d), and Se (4s and 4p). This indicates that the colors and optical band gaps of the $CsLnMSe_3$ materials may be manipulated through a variety of chemical substitutions. In contrast, the

(49) Hybertsen, M. S.; Louie, S. G. *Comments Condens. Matter Phys.* **1987**, *13*, 223−247.
(50) Perrin, M.-A.; Wimmer, E. *Phys. Rev. B: Condens. Matter* **1996**, *54*, 2428−2435.
(51) Pankove, J. I. *Optical processes in semiconductors*; Prentice-Hall: Englewood Cliffs, NJ, 1971.
(52) Axtell, E. A., III; Liao, J.-H.; Pikramenou, Z.; Kanatzidis, M. G. *Chem. Eur. J.* **1996**, *2*, 656−666.
(53) Axtell, E. A., III; Park, Y.; Chondroudis, K.; Kanatzidis, M. G. *J. Am. Chem. Soc.* **1998**, *120*, 124−136.

optical transitions of the MSe binaries are mainly between Se (4p) and M (*n*s and *n*p; $n = 4$ for Zn, 5 for Cd, and 6 for Hg). In these binaries, there is a much larger dispersion of the HOMO and LUMO.

Finally, the red $CsYbZnSe_3$ and $CsCeHgSe_3$ compounds are strikingly different from the other $CsLnMSe_3$ materials. In particular, when viewed along [010] $CsCeHgSe_3$ is red whereas when viewed along [001] it is sufficiently dark, indeed almost black, to make absorption measurements in this direction impossible. All absorption measurements were performed on $CsLnMSe_3$ crystals of similar size and shape. Therefore, the striking dichroism of $CsCeHgSe_3$ is an inherent property and is not an artifact of the shape of those particular crystals. The red color of $CsYbZnSe_3$ and dichroism of $CsCeHgSe_3$ may result from optical transitions involving the 4f orbitals of Yb and Ce. Such transitions were proposed to explain the red color of γ-Ce_2S_3[50,54,55] and the yellow color of $K_3CeP_2S_8$.[56]

Conclusion

Within limits, tuning of the band gaps in the $CsLnMSe_3$ compounds may be achieved by control of chemical composition and crystal orientation. We find that the optical band gaps for the $CsLnMSe_3$ compounds (M = Zn, Cd, Hg) change by as much as 0.69 eV with composition and by as much as 0.20 eV with crystal orientation (Table 6). The precise control of the optical band gap of a material is an important tool for the design of photonics devices, such as optical waveguides[57] and optical filters.[58] These $CsLnMSe_3$ compounds are an interesting and potentially useful class of optical materials.

Acknowledgment. This research was supported by National Science Foundation Grant DMR00-96676, a Ford Predoctoral Fellowship to K.M., and a Northwestern University Presidential Fellowship to C.L.H. Use was made of the Central Facilities supported by the MRSEC program of the National Science Foundation (DMR00-76097) at the Materials Research Center of Northwestern University.

Supporting Information Available: Crystallographic files in CIF format for $CsLnCdSe_3$ (Ln = Ce, Pr, Sm, Gd, Tb, Dy, Y) and $CsLnHgSe_3$ (Ln = La, Ce, Pr, Nd, Sm, Gd, Y). This material is available free of charge via the Internet at http://pubs.acs.org.

IC020733F

(54) Mauricot, R.; Gressier, P.; Evain, M.; Brec, R. *J. Alloys Compd.* **1995**, *223*, 130−138.
(55) Zhukov, V.; Mauricot, R.; Gressier, P.; Evain, M. *J. Solid State Chem.* **1997**, *128*, 197−204.
(56) Gauthier, G.; Jobic, S.; Brec, R.; Rouxel, J. *Inorg. Chem.* **1998**, *37*, 2332−2333.
(57) Joannopoulos, J. D.; Villeneuve, P. R.; Fan, S. *Nature (London)* **1997**, *386*, 143−149.
(58) Dirix, Y.; Bastiaansen, C.; Caseri, W.; Smith, P. *Adv. Mater.* **1999**, *11*, 223−227.